Pyrimidoquinxoalinophenanthroline opens next chapter in design of bridging ligands for artificial photosynthesis

Jannik Brückmann,[a] Carolin Müller,[b,c] Tamar Maisuradze,[b] Alexander K. Mengele,[a] Djawed Nauroozi,[a] Sven Fauth,[a] Andreas Gruber,[d] Stefanie Gräfe,[b] Kerstin Leopold,[d] Stephan Kupfer,[b] Benjamin Dietzek-Ivanšić,*,[b,c] Sven Rau*,[a]

[a] J. Brückmann, A. K. Mengele, S. Fauth, Dr. D. Nauroozi, Prof. Dr. S. Rau, Institute of Inorganic Chemistry I, Ulm University, Albert-Einstein-Allee 11, 89081 Ulm, Germany, E-mail: sven.rau@uni-ulm.de

[b] T. Maisuradze, Dr. C. Müller, Dr. S. Kupfer, Prof. Dr. S. Gräfe, Prof. Dr. B. Dietzek-Ivanšić, Institute of Physical Chemistry ,Friedrich-Schiller University Jena, Helmholtzweg 4, 07743 Jena, Germany

[c] Dr. C. Müller, Prof. Dr. B. Dietzek-Ivanšić, Leibniz Institute of Photonic Technology (IPHT) e.V., Department Functional Interfaces, Albert-Einstein-Straße 9, 07745 Jena, Germany, E-mail: benjamin.dietzek@leibniz-ipht.de

[d] A. Gruber, Prof. Dr. K. Leopold, Institute of Analytical and Bioanalytical Chemistry, Ulm University, Albert-Einstein-Allee 11, 89081 Ulm, Germany

Abstract: Using a dehydrogenative chemistry on the complex approach, a new polypyridine bridging ligand that bridges the gap of already existing systems is synthesized. By the usage of versatile cross-coupling reactions two different coordination spheres are included in the ligand architecture. Due to the twisted geometry of the novel ditopic ligand, the resultant division of the ligand in two distinct subunits leads to steady state as well as excited state properties of the corresponding mononuclear Ru(II) polypyridine complex resembling those of prototype $[Ru(bpy)_3]^{2+}$ (bpy = 2,2´-bipyridine). The localization of the initially optically excited and the nature of the long-lived excited states on the Ru-facing ligand spheres is evaluated by resonance Raman and fs-TA spectroscopy, respectively, and supported by DFT and TDDFT calculations. Coordination of a second metal (Zn or Rh) to the available bis-pyrimidyl-like coordination sphere strongly influences the frontier molecular orbitals apparent by e.g., luminescence quenching. Thus, the new bridging ligand motif offers electronic properties which can be adjusted by the nature of the second metal center. Using the heterodinuclear Ru-Rh complex, visible light-driven reduction of NAD^+ to NADH was achieved, highlighting the potential of this system for photocatalytic applications.

Introduction

Light-induced electron transfer lies at the heart of photosynthesis, the most important chemical transformation process on earth.[1] Within artificial photosynthesis significant steps towards a deeper understanding of structural and electronic factors determining the efficiency of electron transfer rely on the interplay between advanced spectroscopic methods and the availability of suitable model systems.[2–6] Heterooligonuclear metal complexes containing specific bridging ligands (BL) which determine the distance between the (photo)redox active metal centers, the degree of electronic coupling and the stability of the coordination centers utilizing the chelate

effect have been pivotal for this development and yielded the discovery of supramolecular photocatalysts for water splitting.[7–10] Access to fundamentally new bridging ligands is therefore a key requirement to improve our understanding of fundamental aspects of light-induced electron transfer and at the same time enabling new applications in light-driven catalysis. Due to this, bridging systems of high rigidity with bipyridine- or phenanthroline-like coordination spheres providing sufficient stability were evaluated in numerous reports and review articles.[10–13] Representative examples with increasing bridging ligand length would be the row of 2,2'-bipyrimidine (bpm), 1,6,7,12-tetraazaperylene (tape) or eilatin like structure and tetrapyrido[3,2-a:2',3'-c:3'',2''-h:2''',3'''-j]phenazine (tpphz) (as depicted in Figure 1). Several mono- and dinuclear transition metal complexes of those relays have been investigated so far.[9,14–19] Since $[Ru(bpy)_3]^{2+}$-type complexes were extensively studied upon their chemical, photophysical and photochemical properties, fundamental studies on complexes with Ru(II) photosensitizing and bpym (2,2'-bipyrimidine),[18,20–22] tape (tetraazaperylene or dipyrido[4,3,2-de:2',3',4'-gh][1,10]phenanthroline),[14,15,23,24] eilatin[24,25] and tpphz (tetrapyrido[3,2-a:2',3'-c:3'',2''-h:2''',3'''-j]phenazine)[9,17,26] bridging unit were made. For bpym- and tape-like dinuclear complexes relatively strong ground-state coupling between both metal centers has been observed whereas tpphz seems to largely decouple them.[15,20] Photocatalytic hydrogen formation with related Ru-BL-Pd catalysts is only observed with tpphz.[9] However, tpphz utilization is hampered by a low lying phenazine-based accepting orbital severely limiting the choice of reducible catalytic metal centers. Principal access to a bridging ligand with shorter metal-to-metal distances and potentially sufficient degree of electronic decoupling can be derived starting from 5,6-disubstituted 1,10-phenanthroline.

Glazer and Tor presented synthetic concepts for dehydrogenative CC coupling chemistry in related systems,[24] which should enable a route towards the target unit. First, coupling of 5-substituted pyrimidine to a Ru(II) 1,10-phenanthroline system at its 5,6 positions *via* Pd catalysed cross-coupling reactions was performed. This was followed by the built-up of a conformationally rigid bridging ligand *via* Pd on charcoal activated ring-closure procedure reported earlier by Glazer and Tor.[24]

This contribution introduces the synthesis of a novel bridging ligand coordinated to a ruthenium center to bridge the gap between already existing systems. The synthesis is complemented by detailed structural and electronic characterization by optical spectroscopy and quantum chemistry. Furthermore, its ability for coordination of a second metal center i.e., with respect to future applications in the scope of photocatalysis, is explored.

Results and Discussion

The synthesis of Ru(II) polypyridine complexes bearing π-extended, N-heterocycle substituted 1,10-phenanthroline (phen) type ligands was performed *via* two different transition metal catalysed cross-coupling reactions at the dibrominated $RuphenBr_2$-type (i.e. $[(tbbpy)_2Ru(phenBr_2)]^{2+}$; tbbpy = 4,4'-di-*tert*-butyl-2,2'-bipyridine; $phenBr_2$ = 5,6-dibromo-1,10-phenanthroline) precursor and a thermal dehydrogenation reaction using palladium on charcoal (Pd/C).

Starting from the dibrominated, literature-known compound **$RuphenBr_2$** either Suzuki or Stille reactions were used to form the 1,10-phenanthroline-5,6-bis-pyrimidine substituted complex **Rudpymp** ($[(tbbpy)_2Ru(\mathbf{dpymp})]^{2+}$; **dpymp** = 5,6-di(pyrimidin-5-yl)-1,10-phenanthroline). So far, literature examples upon cross-coupling approaches with 5,6-dibromo-1,10-phenanthroline only used electron-rich organometallic derivatives like donor-substituted phenyl or thiophene moieties.[27] Only few articles integrate acceptor-substituted phenyl compounds because monosubstitution and/or dehalogenation reactions hamper those synthetic pathways.[28] Especially, cross-coupling with electron-deficient nitrogen heterocycles proves to be challenging.[29–31] Published reaction conditions for Stille cross-coupling yielded

exclusively in mono-substitution and concomitant dehalogenation of the second halogen substituent.[32–35] Usage of copper iodide additive[36,37] di-substitution leads to **Rudpymp** in a yield of up to 67%. To our own surprise, Suzuki cross-coupling with standard reaction conditions[27] gave excellent yields up to 88%. Purification in both cases was done *via* slow diffusion of diethyl ether into a concentrated solution of **Rudpymp** in acetonitrile.

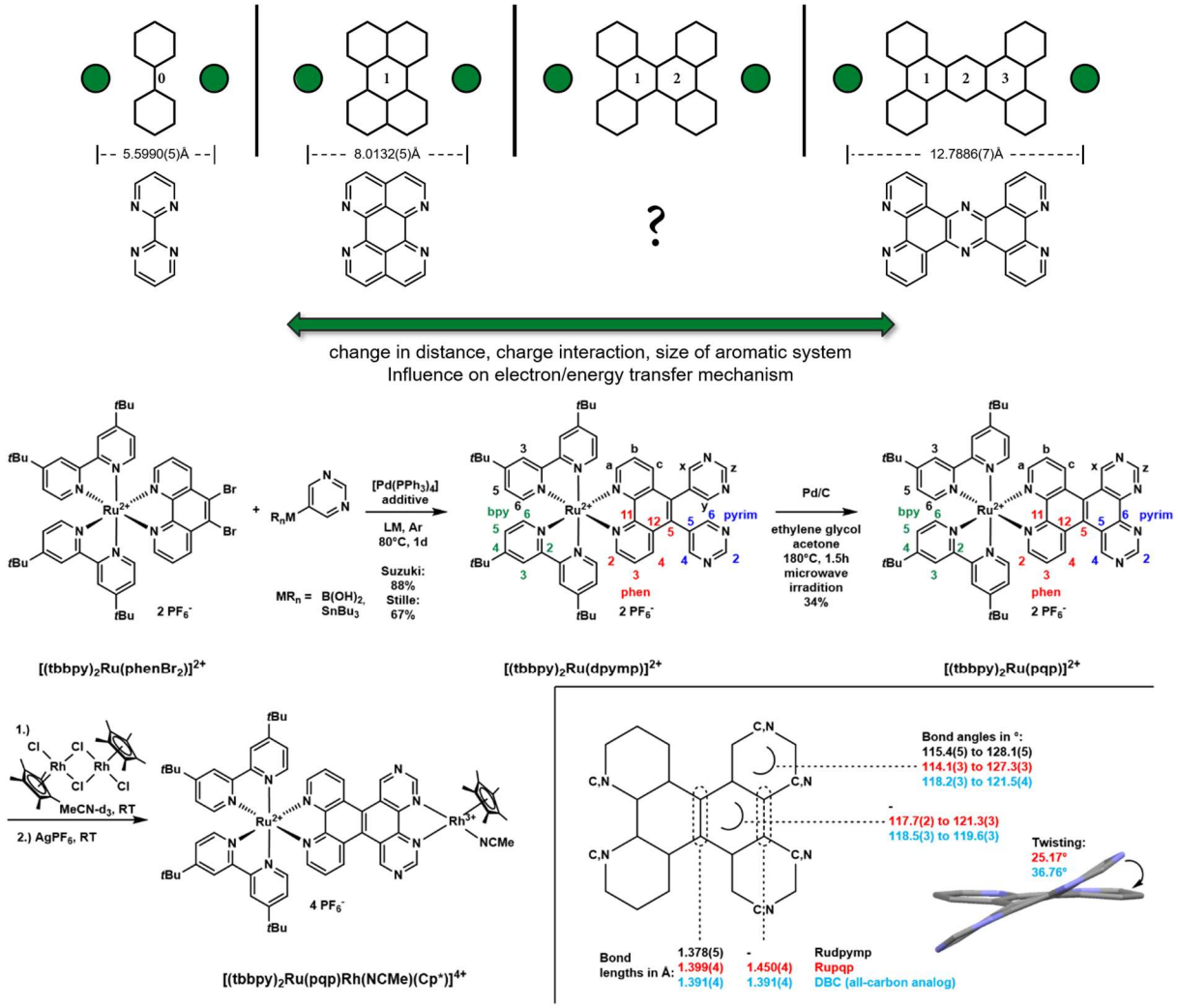

Figure 1. Top: Overview of the existent bridging ligand structures and selected metal-to-metal distances from solid state structures of $[(bpy)_2Ru(bpym)Ir(Cp^*)]^{2+}$,[22] $[(L)RutapeRu(L)]^{4+}$ (with L = N,N'-dimethyl-2,11-diaza-[3.3](2,6)-pyridiophane)[14] and $[(tbbpy)_2RutpphzRu(tbbpy)_2]^{4+}$.[9] Bottom: Synthetic protocol for Suzuki and Stille cross coupling reactions and the following ring closing reaction; positions of the respective protons (in black) and carbon atoms (coloured; with ligand (sphere) abbreviations) were marked; inset shows a part of the all-carbon analog dibenzo[*g,p*]chrysene (DBC) or **pqp** framework and the discussed bond angles and lengths; additionally, a part of the solid-state structure of **Rupqp** is used to visualize the twisting compared to all-carbon DBC derivatives; colour code: **Rudpymp** (black), **Rupqp** (red), DBC (light blue).

To achieve a fully ring-closed system of the bis-pyrimidyl substituted phenanthroline moiety, dehydrogenation reactions were conducted. Literature-known cyclization with Pd/C in ethylene glycol and acetone under elevated temperatures gave an NMR-detectable amount of **Rupqp** ($[(tbbpy)_2Ru(\mathbf{pqp})]^{2+}$; **pqp** = pyrimido[5',4':7,8]quinazolino[5,6-*f*][1,10]phenanthroline). Improving the reaction conditions (additive(s), temperature, time; see chapter 3.4 in SI) and running this reaction in a microwave setup significantly increased yields (from NMR-detectable to 34% yield). Strikingly, the reaction was not possible using **Rudpymp** obtained under Stille

conditions. In total reflection X-ray fluorescence spectroscopy (TXRF) significant residues of copper and iodide could be detected (see Figure S66). To verify that one of these elements prohibits the ring closure reaction, copper iodide was added deliberately to the Suzuki product. As under these conditions the ring-closure reaction failed as well, the inhibiting effect of CuI residues on the cyclization reaction is demonstrated (see Figures S37 and S38).

After the ring closure, **Rupqp** offers a second coordination sphere. This chelating ligand sphere emerges as an electron deficient 4,4'-bipyrimidyl-like environment. To evaluate the ability to attach a second metal center to **Rupqp**, we decided for the typically efficiently introducible Rh(Cp*)(X) (Cp* = pentamethylcyclopentadienyl) fragment. Earlier reports accomplished the coordination by simply stirring both the bridging ligand containing Ru-complex and the Rh(III) dimer in solution of e.g. methanol or methylene chloride, the latter was applied for example for $[(tbbpy)_2Ru(tpphz)]^{2+}$(i.e. $[(tbbpy)_2Ru(tpphz)]^{2+}$).[38,39] Within this work, this attempt yielded only partial conversion. Follow-up purification steps with solvents with (even partial) donor capability, ended in partial chlorido ligand substitution by solvent molecule(s). Due to this ligand lability, earlier described methods were used to cleave the chlorido ligand quantitatively by addition of silver hexafluorophosphate.[40] To exclude insoluble silver chloride, several centrifugations in methylene chloride and subsequent re-crystallization were done. Possibly due to soluble silver clusters as it was shown earlier,[41] atomic absorption spectrometry (AAS) still reveals silver contaminations (see ESI Figure S67).

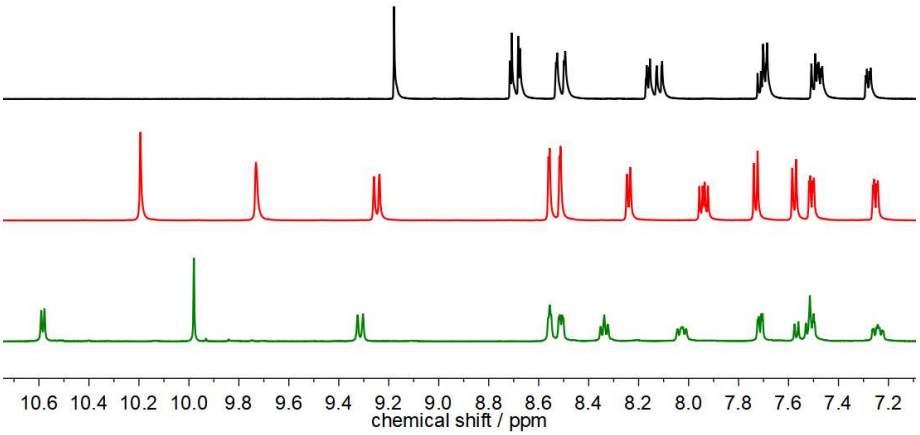

Figure 2. ^{1}H NMR spectra of **Rudpymp** (top), **Rupqp** (middle) and **RupqpRh** (bottom) in acetonitrile-d_3 (400 MHz, due to absence of concentration dependence as shown in Figures S23 and S24 no specific concentrations were used).

For the ^{1}H NMR spectra of **Rudpymp** and **Rupqp**, the signal pattern is simplified upon ring closure from **dpymp** to **pqp** (see Figure 2). This is due to the long-range coupling of protons x and y which causes – in addition to proton z – a second singlet to appear (see Figure 1 for the assignment). All pyrimidine protons and the c protons of the phen (1,10-phenanthroline) sphere are considerably shifting downfield due to the ring-closed system and even further due to coordination of Rh(III). To exclude effects of silver ions, $AgPF_6$ was added to **Rupqp** which does not induce changes in the chemical shifts (see Figure S44). Upon ring closure, changes in the chemical shift of maximal 1.5 ppm (H_x) can be observed. This effect diminishes progressively when moving from the inner ligand sphere to the adjacent phenanthroline/pyrimidyl positions and the peripheral *tert*-butyl-bipyridines. Two possible explanations for this effect might be i) a varied ring current leading to altered deshielding/shielding of the different moieties or their adjacent aromatic rings and/or ii) an enhanced conjugation between phenanthroline and bis-pyrimidyl spheres upon ring closure.[42,43] The latter clearly can be seen in analysing bond lengths and torsion angles within the **pqp** ligand (*vide infra*). The electron poor character of the **pqp** ligand sphere is further enhanced by coordination of Rh(III). Again, changes of the chemical shifts are of significant

level for the nearby pyrimidyl protons and diminishes for the farther apart phen and tbbpy protons.

Compared to complexes bearing shorter (e.g. $[(bpy)_2Ru(tape)]^{2+}$[15]) and longer (e.g. Rutpphz[44]) bridging ligands, **Rudpymp** and **Rupqp** show no concentration dependence in acetonitrile within a concentration range of 1.3 mM to 30.3 or 18.5 mM, respectively (see Figures S23 and S24). The mononuclear complex of tape shows rather small proton chemical shifts (up to 0.29 ppm) in a similar concentration range, but they appear to be too small to calculate a dimerization constant. In high contrast, the tpphz complex exhibits large shifts and consequently high dimerization constants (120 ± 19 M^{-1}).[44] This is surpassed by the eilatin (dibenzo[b,j]-dipyrido[4,3,2-de:2',3',4'-gh][1,10]phenanthroline; 260 M^{-1})[25] and dbneil (dibenzo[b,j]diquinolino[4,3,2-de:2',3',4'-gh][1,10]phenanthroline; 750 M^{-1})[45] complexes of $[(bpy)_2Ru(X)]^{2+}$ type structure.

Single crystal analysis

Suitable crystals for X-ray diffraction analysis were obtained by slow evaporation of appropriate solvent mixtures (for details see SI). The solid-state structures of **Rudpymp** and **Rupqp** shown in Figure 3 reveal typical bite angles of 78.19(9)° to 79.6(1)° for the tbbpy ligands and 78.5(1)° (**Rudpymp**) or 78.33(9)° (**Rupqp**) for the novel ligand moiety. **Rudpymp** exhibits torsion angles of the two pyrimidine units of 70.25° and 62.77° with respect to the phenanthroline plane. The range of the observed torsion angels is in accordance to other σv symmetric systems reported in literature.[28] Medium steric hinderance produced by the x protons (recall Figure 1) of the pyrimidine rings yields less tilted geometries than observed for higher sterically crowded substituents.[32] Hydrogen bonding of one of the pyrimidine nitrogen atoms of **Rudpymp** towards co-crystallized water (1.884 Å) may affect this as well.

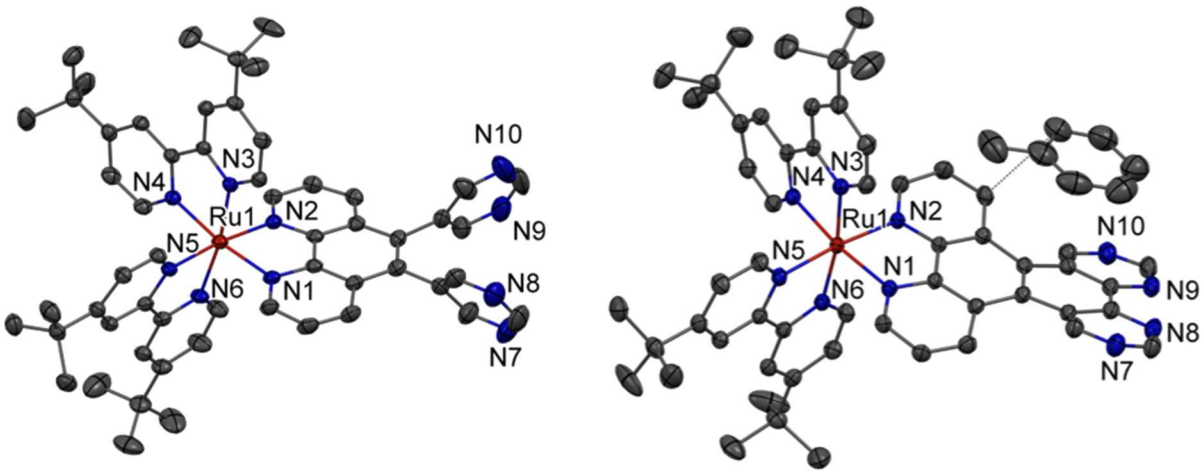

Figure 3. Solid-state structure of **Rudpymp** (left) and **Rupqp** (right) (thermal ellipsoids are drawn at a probability level of 50%). Hydrogen atoms, PF_6^- counter anions and solvent molecules are omitted for clarity; additionally, intermolecular interactions of a toluene molecule with **Rupqp** are depicted.

Upon ring closure, **Rupqp** reveals a conformationally rigid chemical structure where the pyrimidyl units in the backbone are attached to each other directly (see schematic representation in Figure 1). **Rupqp** exhibits shortening of the bonds between the phenanthroline (C5 and C6, see Figure 1) and pyrimidyl units (C5). Bond lengths decrease from 1.490(5) Å and 1.492(5) Å to 1.455(4) Å and 1.459(4) Å, respectively. Additionally, interior angles of the **pqp** ligand deform upon ring closing (range from 114.07° up to 127.34°), whereas

the angles in the new, central sphere are more evenly distributed (from 117.69° up to 121.28°). Similar to DBC (1.388 Å,[46] 1.397 Å[47]), the bond between C5 and C6 of the phenanthroline moiety (1.399(4) Å) is in the range of typical benzene-like sp^2-sp^2 hybridized, aromatic C-C bonds with bond lengths of about 1.40 Å.[42,48] In addition, both **pqp** and DBC reveal a slightly longer bond length (1.450(4) Å) between the aromatic rings in the backbone (each C6 atom of the pyrimidyl units, see Table 1).

Table 1. Comparison of **Rupqp** with literature examples on all-carbon dibenzo[*g,p*]chrysene derivatives; TMS = trimethylsilyl.

Compound	Bond length central ring [Å]	Torsion angles [°]
Rupqp (DFT)	1.399(4) (1.404)	25.17 (29.5)
Dibenzo[*g,p*]chrysene[49,50]	1.388(2)/1.391(4)	38.94
Bis-Pd-dicarbocorrole[47]	1.450(4)	29.95
Tetra-TMS-DBC[51]	1.387(3)	44.95
DBC-Cl_2[52]	1.37(2)	40.65

Possibly due to steric strains between the hydrogens at the x position of the pyrimidine and c of the phenanthroline, a tilted geometry of the **pqp** can be found in the solid-state structure. A torsion angle of 25.17° is observed which is in good agreement with the DFT results (29.5°) (Tables 1 and S5). All-carbon derivatives of the **pqp** ligand with the general structure of dibenzo[*g,p*]chrysene reveal even higher twisting of 29.95-44.95°.[46,47,49,52]

Noteworthy, the **pqp** ligand reveals stacking with co-crystallized toluene solvent molecule with a distance of 3.267(6) Å. Due to this tilting, atropisomerism can be expected, but in one unit cell only an enantiomeric pair of Λ- (chirality at the ruthenium center) with M (chirality at the **pqp** ligand) and Δ-P can be found (see Figures S32-S34).[53] Regardless of the XRD analysis results, atropisomerism which must result from the twisted bridging ligand geometry cannot be excluded as the accompanying diastereomers can remain in solution.

Electrochemistry

In order to determine the electrochemical properties of **Rudpymp**, **Rupqp** and **RupqpRh,** cyclic voltammetry and differential pulse voltammetry experiments were conducted (see Figures 4 and S4.1-S4.6). All three complexes were studied in acetonitrile solutions (1 mM) containing supporting electrolyte of $[Bu_4N][PF_6]$ (0.1 M). The data were referenced against the Fc/Fc^+ (ferrocene/ferricenium) couple and are summarized in Table 2.

Consistent with literature, the reversible Ru(II)/(III) oxidation of both mononuclear complexes appears at 0.81 V (**Rudpymp**) and 0.83 V (**Rupqp**). The Ru(II)/(III) oxidation is insensitive to the peripheral introduction or ring closure of the pyrimidyl moieties.[27] **RupqpRh** exhibits a reversible Ru(II)-based oxidation at anodically shifted potentials of 0.91 V. The four cathodic events of **Rudpymp** are reversible or quasi-reversible. Assuming no effect of the new **dpymp** ligand on the tbbpy ligands, the potentials at -1.95 V and -2.37 V can be assigned to the latter according to literature results.[27] The one-electron reduction of bare 1,3-pyrimidine takes place at rather negative potentials.[54] Hence, we conclude that the first reductive event of **Rudpymp** at -1.67 V is based on the phenanthroline moiety. This reduction is shifted anodically by *circa* 100 to 120 mV compared to similar complexes (see Table 2).[27,55]

Upon ring closure, five reduction events emerge for **Rupqp** (see also DPV in Figure 4). Thus, the fifth reduction is likely localized on the new bridging ligand architecture. Possibly, it can be either ascribed to the novel central sphere within the **pqp** ligand or an accessible, second reduction of the pyrimidine units. The redox events at -1.67 V (**Rudpymp**) or -1.53 V (**Rupqp**) without apparent shifts in the oxidation potential of the Ru(II)/(III) couple decrease the electrochemical band gap – ΔE(**Rudpymp**) = 2.48 eV and ΔE(**Rupqp**) = 2.36 eV – compared to $[Ru(tbbpy)_3]^{2+}$ (ΔE = 2.55 eV). The coordination of the redox active unit, i.e. Rh(Cp*), induces additional changes.

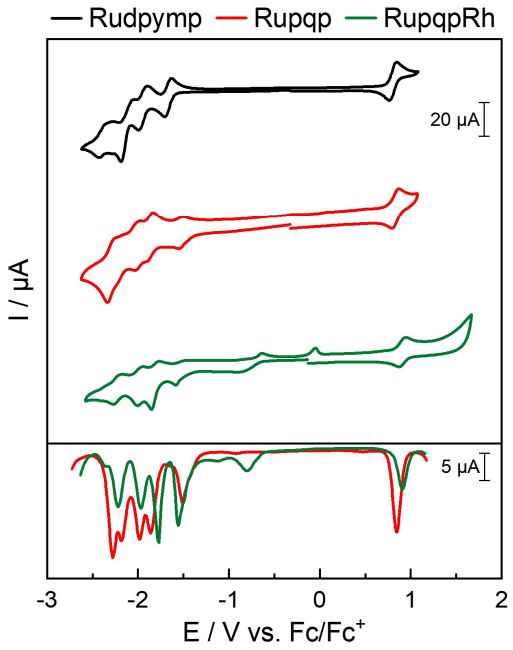

Figure 4. Cyclic voltammograms (top) and differential pulse voltammograms (bottom) of **Rudpymp** (black), **Rupqp** (red) and **RupqpRh** (green) in acetonitrile solution (1 mM) referenced against the ferrocene/ferricenium (Fc/Fc^+) couple. Conditions: scan rate 0.1 mVs^{-1} (black, green), 0.2 mVs^{-1} (red), $[Bu_4N][PF_6]$ at 0.1 M as supporting electrolyte.

First, due to the Rh(III) metal center, two reduction events at -0.80 and -1.12 V appear. They emerge at similar potentials as for the literature-known $[Rh(bpm)(Cp^*)Cl]^+$ (with bpm = 4,4'-bipyrimidine, see Table 2) where a two-fold reduction takes place. In accordance with literature, the rhodium center displays two consecutive reduction steps in case of acetonitrile coordinated species.[56]

Second, all subsequent ligand-based reductions emerge at similar potentials as for **Rupqp**. Only the fifth reduction of **Rupqp** is shifted considerably in **RupqpRh** and lies outside of the accessible potential window or it just appears as the small shoulder visible at high cathodic potentials in the CV and DPV (see Figure 4). Interestingly, the Ru(II)/(III) oxidation shifts anodically by 80 mV. This hints to a more electron deficient Ru(II) center comparable to $[(bpy)_2Ru(bpm)]^{2+}$ ($E_{1/2ox}$ = 1.05 V). Alternatively, an increased influence of the Rh(III) metal center due to the shorter bridging ligand can be considered. For Rutpphz and RutpphzRh ($[(tbbpy)_2Ru(tpphz)Rh(Cp^*)Cl]^{3+}$) only a 30 mV anodic shift was observed due to coordination of Rh(III).[38]

Regardless of the anodically shifted Ru oxidation, **RupqpRh** still shows smaller electrochemical bandgap properties of the **Rupqp** part (ΔE = 2.47 eV) compared to $[(tbbpy)_3Ru]^{2+}$. Since related 5,6-substituted complexes show a comparable effect without any changes in their photophysics,[32,57] steady-state absorption and emission properties of **Rudpymp** and especially **Rupqp** and **RupqpRh** were studied (*vide infra*).

Table 2. Electrochemical and spectroscopic properties of **Rudpymp**, **Rupqp** and **RupqpRh** together with suitable substances for comparison. * shoulder

Compound	**$E_{1/2ox}$ / V**	**$E_{1/2red}$ / V**	**λ(abs,max)$\lambda_{abs,max}$ / nm (ε [10^3 $M^{-1}cm^{-1}$])**	**λ(em,max) / nm**	**Φ(em, Ar)/Φ(em, air)**
$[(tbbpy)_3Ru]^{2+}$[27,57]	0.73	-1.82, -2.02, -2.28	451 (13)	607	9.5% / 1.8%
$[(tbbpy)_2Ru(phen)]^{2+}$[55]	0.74	-1.77, -1.98, -2.25	454 (16.0)	610	-
$[(tbbpy)_2Ru(phenBr_2)]^{2+}$[27]	0.85	-1.79, -2.00, -2.32	449 (14.3)	631	-
Rudpymp	0.81	-1.67, -1.95, -2.18, -2.37	451 (19.1), 336 (8.16), 285 (78.2)	631	16% / 1%
Rupqp	0.83	-1.53, -1.86, -2.01, -2.19, -2.29	452 (18.8), 336 (17.4), 282 (117)	637	12% / 1%
RupqpRh	0.91	-0.80, -1.12,* -1.56, -1.77, -1.97, -2.22, -2.36*	542, 451, 336, 285	637	2% / 0%
$[Rh(bpm)(Cp^*)(Cl)]^+$[58]		-0.92	375, 364	-	-

Characterization of the Franck-Condon region

To elucidate the impact of the p-extension of the 1,10-phenanthroline (phen) moiety by a single-bond (**Rudpymp**) or ring-annulation strategy (**Rupqp**) on the Franck-Condon region, we employ steady state absorption and resonance Raman (rR) spectroscopy as supported by TDDFT simulations. The discussion starts on the absorption properties of **Rudpymp** and **Rupqp** and subsequently turns to the rR data collected upon 405 and 473 nm excitation.

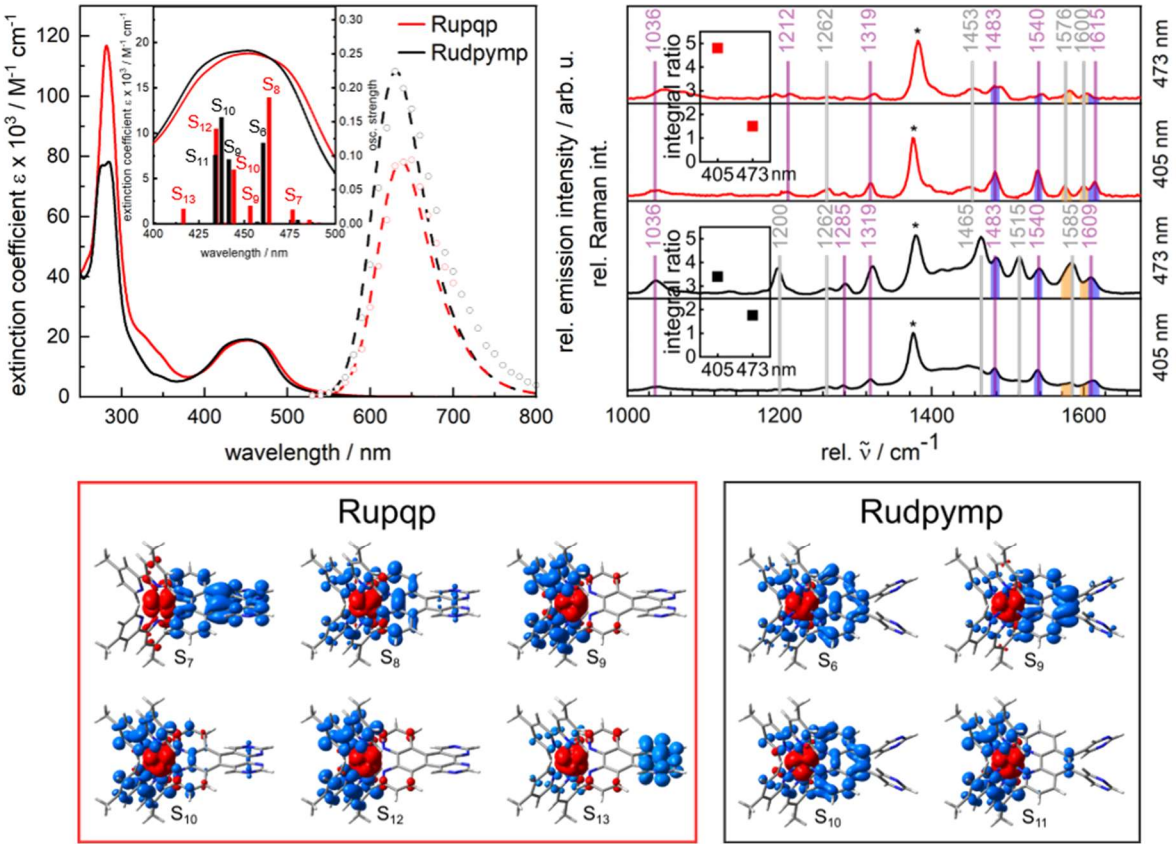

Figure 5. Top left: Extinction coefficients of **Rudpymp** (black) and **Rupqp** (red) with relative emissions (dashed) intensities (OD 0.1 at 451 nm, λ(ex) = 451 nm), electronic transitions underlying the absorptions bands as obtained at the time-dependent density functional level of theory are indicated in the inlet; top right: resonance Raman spectra of **Rudpymp** (bottom) and **Rupqp** (top) upon 405 nm (bottom) and 473 nm (top) excitation in acetonitrile. The tbbpy-, and **dpymp-** or **pqp-**type modes are indicated by violet and grey bars, respectively. The integral ratios of selected modes (tbbpy in light blue relative to **dpymp**/**pqp** in light orange) for the respective excitation wavelength are included as insets for **Rupqp** (red) and **Rudpymp** (black); integral values are normalized to the integral of the modes of Rudpymp upon excitation with 405 nm, respectively; bottom: charge density differences visualizing main electronic transitions contributing to the electronic absorption of **Rudpymp** and **Rupqp** in the visible region; charge transfer takes place from red to blue.

UV/vis absorption.

The absorption spectrum of the bis-pyrimidyl substituted complex **Rudpymp** shows three major features: a narrow and strong absorption band at 286 nm (78.2 × 10^3 $M^{-1}cm^{-1}$), a weaker shoulder between 300 and 380 nm and a broad, featureless metal-to-ligand charge-transfer (MLCT) absorption band with a maximum at 451 nm (19.1 × 10^3 $M^{-1}cm^{-1}$). Such spectra are typical for $[(tbbpy)_2Ru(phen)]^{2+}$-type complexes, *i.e.*, where the phen-moiety is substituted in the 5- and 6-position.[27,32] The underlying transitions are composed of bpy- and phen-centered π-π* (260 – 380 nm, bpy: S_{57} and S_{58}, phen: S_{66}) and MLCT transitions (380 – 550 nm, $MLCT_{dpymp}$: S_6 and S_9, $MLCT_{bpy}$: S_{10} and S_{11}, see Table S8.2 and Figure S8.1).

Although the difference between oxidation and reduction potentials in **Rudpymp** (2.48 eV, see Table 2) is smaller than in the parent complex $[(tbbpy)_2Ru(phen)]^{2+}$ (2.58 eV), the MLCT absorption maxima of both complexes are at around 450 nm. This apparent mismatch between

the electrochemical data (band gap of 2.48 eV, 500 nm) and the spectroscopic findings indicates the presence of multiple low- energy acceptor orbitals on the **dpymp** ligand,[60] which participate in the electrochemical process but have vanishing oscillator strengths in the respective MLCT transitions, e.g. S_1 of $MLCT_{dpymp}$ character at 2.38 eV (520 nm, f = 0.001). Hence, the $MLCT_{bpy}$ and $MLCT_{phen}$ transitions dominate the absorption spectrum of **Rudpymp**, explaining the similarity to the absorption data of $[(tbbpy)_2Ru(phen)]^{2+}$.

Upon ring closure, the molar absorptivity of the MLCT absorption band remains essentially unchanged, while the band at 280 nm (increase by a factor of 1.5) and the shoulders between 300 and 380 nm (increase by a factor of 2.1) become more prominent.

TDDFT simulations associate the enhanced absorption band at *circa* 280 nm with the increased oscillator strength of the π-π* excitation of the **pqp** ligand upon ring C-C bond formation (**Rupqp**: S_{58}, f = 0.514 versus **Rudpymp**: S_{66}, f = 0.371). The MLCT band maximum of **Rupqp** is not shifted with respect to **Rudpymp** (HOMO-LUMO gap of 2.36 eV), which is counterintuitive in view of the ring-annulated π-extension of the phen-ligand, *i.e.*, in comparison to Rudape ($[(bpy)_2Ru(dape)]^{2+}$, dape = diazaperylene),[24] Rutape ($[(bpy)_2Ru(tape)]^{2+}$)[14,15,24] or Rueilatin ($[(bpy)_2Ru(eilatin)]^{2+}$)[25] where significant bathochromic shifts of the MLCT absorption bands have been observed.[14,15,25] In contrast to these shorter π-extended ligands, **Rupqp** reveals a non-planar **pqp** ligand potentially decreasing π-conjugation. The quantum chemical calculations associate the MLCT band in **Rupqp** with low-lying $MLCT_{pqp}$ excitations (into S_7 and S_8) and higher-lying $MLCT_{bpy}$ (into S_{10} and S_{12}) excitations. Like for **Rudpymp**, the low-energy MLCT excitations have vanishing oscillator strengths (*e.g.* S_1, at 2.36 eV, f = 0.001, see Table S8.4). Consequently, the shape and position of the MLCT absorption band of **Rupqp** is similar to **Rudpymp** or the homoleptic reference complex $[Ru(tbbpy)_3]^{2+}$.

Resonance Raman.

To further explore the multiple MLCT transitions, rR spectra were collected upon excitation in the red and blue flank of the MLCT absorption band, *i.e.*, at 405 and 473 nm (see Figure 5)[61]. The rR spectra of **Rudpymp** collected upon 405 and 473 nm excitation are composed of modes associated to the tbbpy ligands as well as the phen- and pyrimidyl units of the **dpymp** ligand, respectively. By direct comparison to the homoleptic reference compound $[Ru(tbbpy)_3]^{2+}$ and the parental complex $[(tbbpy)_2Ru(phen)]^{2+}$, we assign the modes at 1036, 1319, 1483, 1540 and 1609 cm^{-1} to the tbbpy ligand sphere. The vibrations centered at 1515 and 1585 cm^{-1} are assigned to phen-associated modes.[62,63] The rR modes at 1200, 1262 and 1465 cm^{-1} are assigned to the pyrimidyl sphere (py), indicating the population of $MLCT_{py}$ states. Thus, the rR data supports the initial excitation – as provided by TDDFT – of $MLCT_{bpy}$ as well as two low-lying MLCT states ($MLCT_{phen}$ and $MLCT_{py}$) on the **dpymp** ligand, respectively. The $MLCT_{phen}$ gain in relative weight compared to $MLCT_{tbbpy}$ states upon shifting the excitation wavelength from 405 to 473 nm, which agrees with the TDDFT results (see Figure 5).

The rR spectra of **Rupqp** exhibit similar vibrational modes associated with the tbbpy (1036, 1212, 1319, 1483, 1540, 1615 cm^{-1}) and **pqp** ligand (1262, 1543, 1576 and 1600 cm^{-1}). In direct comparison to **Rudpymp**, the phen-type modes at 1515 and 1585 cm^{-1} vanish (473 nm excitation). However, the integral ratio of the tbbpy-to-**dpymp/pqp**-type modes (between 1470 and 1620 cm^{-1}) is approximately 1.5 for both, **Rudpymp** and **Rupqp** at 473 nm excitation. This indicates similar contributions of the phen acceptor orbital to the Franck-Condon region. Consistent with **Rudpymp**, the contribution of the **pqp** ligand to the formation of the initially excited states increases upon shifting the excitation wavelength from 405 to 473 nm. This is reflected in the decrease of the ratio taken between the integral of the tbbpy (1483, 1540, 1615 cm^{-1}) and **pqp**-type (1576 and 1600 cm^{-1}) modes by a factor of *circa* 2 (see Figure 5). TDDFT supports this trend, revealing low-lying MLCT states with pyrimidyl acceptor orbitals (*e.g.* S_7, see Figure 5).

Characterization of the long-lived excited states.

The long-lived excited states are explored by steady-state and time-resolved emission spectroscopy. The emission band maximum of **Rudpymp** (upon 420 nm excitation) is located at 631 nm, which is red-shifted with respect to the parental complex $[(tbbpy)_2Ru(phen)]^{2+}$ (610 nm) but agrees with $[(tbbpy)_2Ru(phenBr_2)]^{2+}$ (631 nm). This indicates that the pyrimidyl substituents influence the π-system of the phen system.[32]

Upon ring-closure (forming **Rupqp**), the emission maximum is shifted bathochromically by 18 meV to 637 nm. In addition, the comparably high emission quantum yield of 16% for **Rudpymp** decreases to 12% (**Rupqp**) (see Figure 5, black to red). DFT allows to assign the emissive state in both **Rudpymp** and **Rupqp** to a $^3MLCT_{phen}$ (**dpymp**: 647 nm, 1.92 eV, **pqp**: 657 nm, 1.89 eV) , respectively, while the slight bathochromic shift (DFT: 30 meV) is associated with the increased π-system upon C-C bond formation (Figure S89).

The respective emission lifetimes of the complexes are 140 ns (**Rudpymp**) and 170 ns (**Rupqp**, 420 nm excitation in aerated acetonitrile). Overall, the findings indicate that both, **Rudpymp** and **Rupqp**, show emission from a long-lived ^{3}MLCT state, with excess electron density in the proximal ligand sphere, *i.e.*, on the tbbpy ligands and the phen moiety of **dpymp** and **pqp**, respectively. The triplet nature of the lowest-lying excited state is corroborated by its sensitivity to oxygen (see Figures S52 and S53). Emission intensities of both complexes decrease significantly upon aeration (Φ(em) = 1% for **Rudpymp** and **Rupqp**).

Photoinduced dynamics.

To explore the formation of the long-lived ^{3}MLCT state in **Rudpymp** and **Rupqp** ultrafast transient absorption (fs-TA) spectra were collected upon 400 nm excitation The transient absorption spectra of **Rudpymp** and **Rupqp**, collected in acetonitrile, reveal a strong ground-state bleach (GSB) between 400 and 500 nm (the red dashed line reflects the inverted steady-state absorption spectra of the complexes in Figure 6). This GSB is accompanied by strong excited-state absorption (ESA) centered at 350 nm (**Rudpymp**) or 340 nm (**Rupqp**) as well as broad, spectrally flat ESA at wavelengths longer than 510 nm. The latter features are typically observed for Ru-trisbipyridyl-type complexes and are associated with π-π* transitions on the reduced tbbpy and phen moieties and ligand-to-metal charge-transfer (LMCT) transitions (> 500 nm).

In **Rudpymp**, the ESA between 510 and 560 nm is more pronounced than in **Rupqp**. The assignment of ESA features can be supported by TD-DFT calculated dipole and spin-allowed transitions of the relaxed triplet states (^{3}MLCT): The predictions reveal that the ESA of the long-lived ^{3}MLCT excited-states of **Rudpymp** and **Rupqp**, mainly stems from π-π* and LMCT transitions. Moreover, TD-DFT supports the absence of bridge-centered ππ* states which are typically found for structurally related complexes like Rutpphz.[64–66] This hints towards a higher contribution of the phen moiety on the formation of the excited states in **Rudpymp** compared to **Rupqp** and agrees with the rR spectroscopic findings, revealing strong phen-type vibrational modes for **Rudpymp**, which are absent in the rR spectra of **Rupqp**.

For both complexes the decay of the sub-ns signals is best described by two characteristic time constants, namely τ_1 = 2.2 ps and τ_2 = 134 ps (**Rudpymp**) or τ_1 = 2.5 ps and τ_2 = 181 ps (**Rupqp**), respectively. The corresponding decay associated spectra (DAS) of both, **Rudpymp** and **Rupqp**, are qualitatively identical. Hence, we will discuss the excited-state relaxation of both complexes in the framework of the same model.

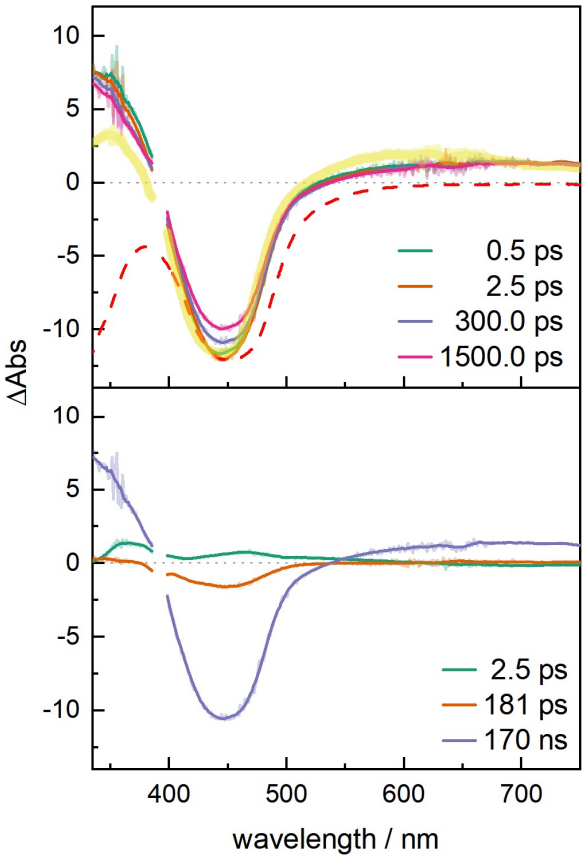

Figure 6. Ultrafast transient absorption (top) and decay-associated spectra (bottom) of **Rupqp**. The red, dashed line in the upper panel shows the scaled and inverted ground state absorption spectrum. For comparison the transient absorption spectrum of **Rudpymp** collected at a delay time of 1.5 ns is shown in yellow. The spectra are collected upon 400 nm excitation (excitation densities of *circa* 5%) in a delay time range between 0.3 and 2 ns in acetonitrile. The lifetime of the long-lived state is obtained from nanosecond time-resolved emission spectroscopy (see Figure S70 and S71).

The spectral changes associated with τ_1, as reflected in DAS(τ_1), are associated with intersystem crossing and vibrational cooling of the initially populated MLCT states.[67–70] This is manifested in the decay of ESA at around 380 nm, associated with ππ* transitions on the reduced tbbpy ligands. This causes a blue-shift of the ESA below 400 nm, accompanied by an increase in the negative signal region. As a result of the processes associated with τ_1, a thermalized ^{3}MLCT with excess electron density localized on the phen moiety is formed. t_2 describes the subsequent formation of the long-lived ^{3}MLCT state. This process is associated with at best minute spectral changes in the ESA, however, a partial recovery of GSB features between 400 and 500 nm is observed.

We associate these findings with a non-radiative decay of a subset of both, ^{3}MC (metal-centered) and ^{3}MLCT$_{py}$ states as typically observed for π-extended [(tbbpy)$_2$Ru(phen)]$^{2+}$-type complexes.[71–75] Ultimately, a long-lived excited ^{3}MLCT state, with excess electron density on the tbbpy ligands (**Rupqp**) or both, the phen and tbbpy moieties (**Rudpymp**) is populated by the process associated with τ_2. These increased contributions of the phen moiety on long-lived excited state agrees with the blue-shift of the emission maximum of **Rudpymp** compared to **Rupqp**.

pqp as bridging ligand – formation of dinuclear complexes and explorative light-driven redox catalysis.

After ensuring the $[Ru(bpy)_3]^{2+}$-like excited-state dynamics of **Rudpymp** and **Rupqp**, the effect of coordinating a second metal center at the new coordination sphere of **Rupqp** was examined. Upon coordination of the [Rh(III)(Cp*)(X)] moiety to the bridging ligand complex **Rupqp** a shoulder at 520 nm emerges in the absorption spectrum which is in line with quantum chemical calculations (Figure S85). Molecular orbitals available for $MLCT_{pqp}$ transitions at long wavelengths (S_6 in Table S11) from Ru(II) to the pq-sphere of the **pqp** ligand are energetically stabilized (2.26 eV) compared to **Rupqp** (2.55 eV). Possibly due to high contributions of the bis-pyrimidyl moiety, the excited state subsequently deactivates radiationless by electron transfer to the appended Rh(III) center. Compared to the ring-closed **Rupqp** coordination of Rh leads to further attenuation of the emission quantum yield from 12% (**Rupqp**) to 2% (**RupqpRh**) (see Figure 7, red to green).

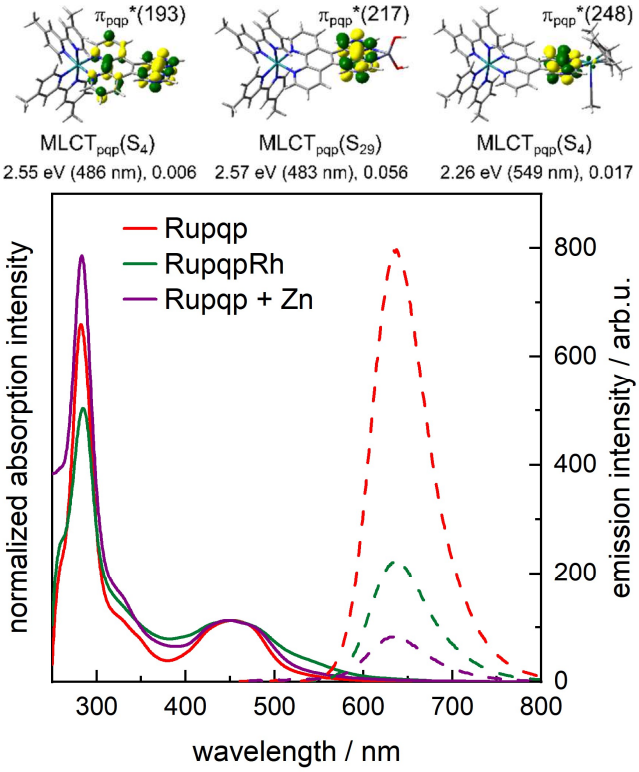

Figure 7. Top: excitation energies, wavelengths and oscillator strengths of low-lying $MLCT_{pqp}$ excitations and involved π_{pqp}* for **Rupqp** (S_4), **RupqpZn** (S_{29}) and **RupqpRh** (S_4); bottom: absorption and emission spectra of **Rupqp**, **RupqpRh** and **Rupqp** + $[Zn(BF_4)_2]$; absorption spectra were normalized at 451 nm; emission spectra were recorded upon excitation at 451 nm (OD 0.1).

Similarly, addition of redox-inactive $Zn(BF_4)_2$ to **Rupqp** induces emission quenching (see Figure 7) as has been observed for Rutpphz complexes.[76,77] Opposite to Rh(III), Zinc(II) induces inverse changes in the frontier molecular orbitals of ground and excited states associated with the **pqp** ligand (see Figures 7 and S83 and S88; MO in Figure 7 is located at slightly higher energies than for **Rupqp**), *i.e.* with the spindensity of the lowest triplet state centered on the Ru(III) and the adjacent phen-sphere. Possibly, the predominant excited state localization on the phen part of the **pqp** ligand enhances charge recombination and thus effective quenching of the ^{3}MLCT emission occurs. From both Rh(III) and Zn(II) coordination it becomes clear that the order of the frontier molecular orbitals of **Rupqp** can be altered depending on the respective second metal center. Thus, the **pqp** appears to be split into two halves with either phen and/or pyrimidyl contributions. Compared to the situation with **Rupqp**,

addition of Zn(II) to **Rudpymp** does not alter absorption or emission behaviour (see Figure S55 and S56). Consequently, the ring closure is required for the interaction with a second metal center.

Finally, the dinuclear complex **RupqpRh** was investigated for the possibility of redox catalysis. Due to the silver contamination found by AAS, all catalytic experiments were accompanied by exclusion experiments with addition of $AgPF_6$.

First, the principal ability of the RhCp* fragment to run formate-driven, chemical catalysis by reduction of the nicotinamide co-factor NAD^+ was investigated (see mechanism reported in literature[78,79]). To further exclude an effect of the mononuclear complex on the reduction to NADH, **Rupqp** was investigated as well. A water/acetonitrile (4:1, *v*:*v*) solution of formate (50 mM) and the respective complex (5 µM) was mixed with 40 eq. of NAD^+. Upon thermal activation (room temperature, 40°C, 50°C), only **RupqpRh** shows conversion of NAD^+ to NADH (visible by the increasing absorbance at 340 nm with εε(NADH) = 6300 $M^{-1}cm^{-1}$[80] and an increasing emission intensity at about 460 nm). As depicted in Figure 8, with increasing temperature, the catalysis is significantly faster. Interestingly, the thermal redox catalysis reaches a plateau already at about 50% conversion.

As the rhodium center offers the possibility to run redox catalysis, the dinuclear complex was subjected to conditions where the catalytically competent Rh(I) intermediate can be formed photochemically (excitation with 470 nm, 50 $mWcm^{-2}$). As it can be seen in Figure S93, the two-fold reduced **Ru(II)pqpRh(I)** dyad can be built up upon illumination (470 nm, 40-50 $mWcm^{-2}$). The band is bathochromically shifted by about 50 nm compared to $[(tbbpy)_2Ru(tpphz)Rh(Cp^*)]^{2+}$ due to the more electron withdrawing nature of the **pqp** ligand.[38] As light-induced reduction was successful with **RupqpRh**, electron transfer from Ru towards Rh can be expected.

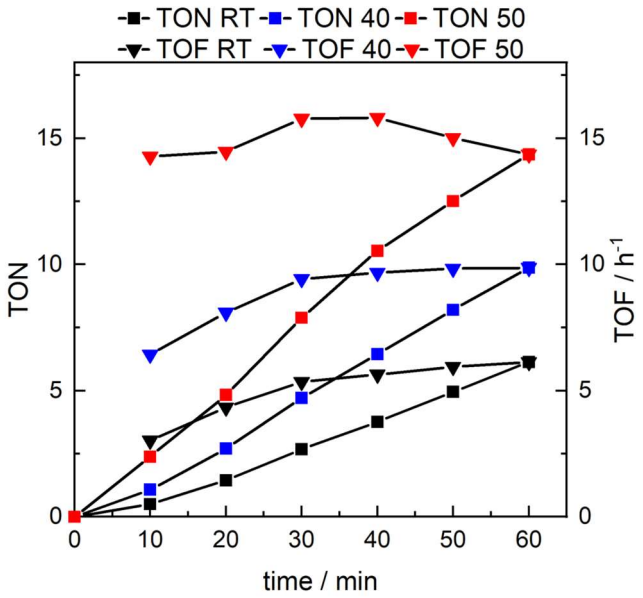

Figure 8. Light-induced redox catalysis of **RupqpRh** at room temperature (black), 40°C (blue) and 50°C (red) in water/acetonitrile mixtures (4:1, *v*:*v*); concentrations used **RupqpRh** (5 µM), NAD^+ (200µM), TEA (0.12 M) and NaH_2PO_4 (0.1 M), excitation with 470 nm (50 $mWcm^{-2}$).

Lastly, we examined if the light-driven Rh(III)/(I) conversion can be accompanied with the reduction of nicotinamide co-factor NAD^+. In phosphate-buffered solution containing triethylamine as electron donor, the dyad **RupqpRh** was irradiated with blue light. Conversion of NAD^+ to NADH was again checked by absorption and emission spectroscopy. **RupqpRh** again was the only catalytically active compound tested in this series of experiments. All other exclusion experiments revealed either radical-mediated product formation of NAD_2[81] by **Rupqp** or **Rupqp** with addition of silver hexafluorophosphate or no conversion for $[Ru(tbbpy)_3]^{2+}$ (see ESI, Figure S98). With elevated temperatures, the conversion with **RupqpRh** is progressively enhanced. An increase in turnover number from 5 (RT) to 10 (40°C) and 15 (50°C) can be observed.

Experimental Section.

For detailed information see the Supporting Information: experimental and synthetic details, structural characterization *via* NMR, mass spectrometry, single-crystal X-ray diffraction, reaction screening, electrochemical characterization, emission lifetimes, steady-state and transient spectroscopy, qualitative element analysis by TXRF and GFAAS and quantum chemical simulations.

Deposition numbers CCDC 2111036 (for **Rudpymp**) and 2111037 (for **Rupqp**) contain the supplementary crystallographic data for this paper. These data are provided free of charge by the joint Cambridge Crystallographic Data Centre and Fachinformationszentrum Karlsruhe *via* www.ccdc.cam.ac.uk/structures.

Conclusion

Pyrimidoquinxoalinophenanthroline, **pqp**, has been synthesized and proven to function as a new bridging ligand fostering light-driven catalysis. This novel bridging ligand was accessed *via* a dehydrogenative chemistry on the Ru-complex approach fusing two pyrimidine spheres *via* a geminate C-C-bond. The respective pyrimidine units were introduced to a Ru(II) 5,6-dibromo-1,10-phenanthroline moiety using Suzuki or Stille cross coupling beforehand. From a structural point of view, the resultant Ru polypyridine complex **Rupqp** fills the gap of previously reported tape- and tpphz-based systems as it exhibits two central aromatic rings rather than one or three, respectively. Due to the twisted nature of the novel bridging ligand that has been revealed by scXRD as well as DFT methods, the steady-state as well as the excited-state properties resemble those of prototype $[Ru(bpy)_3]^{2+}$. This is explained by theoretical investigations and detailed, time-resolved photophysical studies, suggesting a subdivision of the **pqp** bridging ligand into two weakly coupled subunits. However, the energetics of the orbitals on the **pqp** ligand can be significantly influenced by coordination of a second metal center. The coordination of both, Zn(II) and Rh(III), lead to a quenching of the luminescence due to a redistribution of the frontier molecular orbitals as revealed by quantum chemistry. Furthermore, the introduction of Rh(III)(Cp*) leading to **RupqpRh** renders access to visible light-driven photocatalytic reduction of naturally occurring nicotinamide NAD^+ to NADH. These promising results point towards a coordination-induced switching of excited-state localization of **Rupqp**. As the nature of the coordinated metal determines the location of excited states to a large degree, further exploitation towards tuneable photocatalysis will be possible.

Acknowledgements

J.B., C.M., A.K.M., S.G., S.K., B.D. and S.R. gratefully acknowledge the funding by the *Deutsche Forschungsgemeinschaft* (DFG, German Research Foundation) – Projektnummer 364549901 – TRR 234 [A1 and C5]. J.B. is thankful for financial support by the *Fonds der Chemischen Industrie* (*FCI*) for a *Kekulé-Stipendium*. T.M. thanks the *Deutscher Akademischer Austauschdienst* (DAAD, German Academic Exchange Service) for a study scholarship for graduates (91733810). The authors gratefully acknowledge Andrea Hainthaler (Friedrich-Schiller University Jena) for the time-resolved emission measurements, Ilse Friedländer for rR measurements (Friedrich-Schiller University Jena) and Dominik Blaimer (Ulm University) for GFAAS measurements of Ag.

References

[1] W. W. Fischer, J. Hemp, J. E. Johnson, *Annu. Rev. Earth Planet. Sci.* **2016**, *44*, 647–683.

[2] D. F. Harrison, E. Weissberger, H. Taube, *Science (80-.).* **1967**, *159*, 320–322.

[3] C. Creutz, H. Taube, *J. Am. Chem. Soc.* **1969**, *91*, 3988–3989.

[4] C. Creutz, H. Taube, *J. Am. Chem. Soc.* **1973**, *95*, 1086–1094.

[5] G. M. Tom, C. Creutz, H. Taube, *J. Am. Chem. Soc.* **1974**, *96*, 7827–7829.

[6] V. Balzani, G. Bergamini, F. Marchioni, P. Ceroni, *Coord. Chem. Rev.* **2006**, *250*, 1254–1266.

[7] L. De Cola, F. Barigelletti, V. Balzani, P. Belser, A. von Zelewsky, C. Seel, M. Frank, F. Vögtle, *Coord. Chem. Rev.* **1991**, *111*, 255–260.

[8] H. Ozawa, M. A. Haga, K. Sakai, *J. Am. Chem. Soc.* **2006**, *128*, 6–10.

[9] S. Rau, B. Schäfer, D. Gleich, E. Anders, M. Rudolph, M. Friedrich, H. Görls, W. Henry, J. G. Vos, *Angew. Chemie - Int. Ed.* **2006**, *45*, 6215–6218.

[10] G. F. Manbeck, K. J. Brewer, *Coord. Chem. Rev.* **2013**, *257*, 1660–1675.

[11] M. Schulz, M. Karnahl, M. Schwalbe, J. G. Vos, *Coord. Chem. Rev.* **2012**, *256*, 1682–1705.

[12] G. Li, D. Zhu, X. Wang, Z. Su, M. R. Bryce, *Chem. Soc. Rev.* **2020**, *49*, 765–838.

[13] S. Serroni, S. Campagna, F. Puntoriero, C. Di Pietro, N. D. Mc Clenaghan, F. Loiseau, *Chem. Soc. Rev.* **2001**, *30*, 367–375.

[14] T. Brietzke, W. Mickler, A. Kelling, U. Schilde, H. J. Krüger, H. J. Holdt, *Eur. J. Inorg. Chem.* **2012**, 4632–4643.

[15] T. Brietzke, W. Mickler, A. Kelling, H. J. Holdt, *Dalt. Trans.* **2012**, *41*, 2788–2797.

[16] M. G. Pfeffer, T. Kowacs, M. Wächtler, J. Guthmuller, B. Dietzek, J. G. Vos, S. Rau, *Angew. Chemie - Int. Ed.* **2015**, 6627–6631.

[17] M. G. Pfeffer, B. Schäfer, G. Smolentsev, J. Uhlig, E. Nazarenko, J. Guthmuller, C. Kuhnt, M. Wächtler, B. Dietzek, V. Sundström, S. Rau, *Angew. Chemie - Int. Ed.* **2015**, *54*, 5044–5048.

[18] S. Ernst, V. Kasack, W. Kaim, *Inorg. Chem.* **1988**, *27*, 1146–1148.

[19] R. A. Pavinato, J. A. Walk, M. E. McGuire, *Inorg. Chem.* **1993**, *32*, 4982–4984.

[20] D. P. Rillema, K. B. Mack, *Inorg. Chem.* **1982**, *21*, 3849–3854.

[21] M. Hunziker, A. Ludi, *J. Am. Chem. Soc.* **1977**, *99*, 7370–7371.

[22] K. R. Brereton, C. L. Pitman, T. R. Cundari, A. J. M. Miller, *Inorg. Chem.* **2016**, *55*, 12042–12051.

[23] A. Chouai, S. E. Wicke, C. Turro, J. Bacsa, K. R. Dunbar, D. Wang, R. P. Thummel, *Inorg. Chem.* **2005**, *44*, 5996–6003.

[24] E. C. Glazer, Y. Tor, *Angew. Chemie* **2002**, *114*, 4194–4198.

[25] D. Gut, A. Rudi, J. Kopilov, I. Goldberg, M. Kol, *J. Am. Chem. Soc.* **2002**, *124*, 5449–5456.

[26] J. Bolger, A. Gourdon, E. Ishow, J.-P. Launay, *Inorg. Chem.* **1996**, *35*, 2937–2944.

[27] A. Stumper, T. D. Pilz, M. Schaub, H. Görls, D. Sorsche, K. Peuntinger, D. Guldi, S. Rau, *Eur. J. Inorg. Chem.* **2017**, *2017*, 3799–3810.

[28] F. Doettinger, Y. Yang, M. A. Schmid, W. Frey, M. Karnahl, S. Tschierlei, *Inorg. Chem.* **2021**, *60*, 5391–5401.

[29] K. L. Billingsley, K. W. Anderson, S. L. Buchwald, *Angew. Chemie* **2006**, *118*, 3564–3568.

[30] N. Kudo, M. Perseghini, G. C. Fu, *Angew. Chemie - Int. Ed.* **2006**, *45*, 1282–1284.

[31] L. C. Campeau, K. Fagnou, *Chem. Soc. Rev.* **2007**, *36*, 1058–1068.

[32] J. Brückmann, A. A. Heidecker, D. Popovic, A. K. Mengele, D. Nauroozi, P. Bäuerle, S. Rau, *Eur. J. Inorg. Chem.* **2019**, *2019*, 1832–1838.

[33] S. Monro, C. G. Cameron, X. Zhu, K. L. Colón, H. Yin, T. Sainuddin, M. Hetu, M. Pinto, A. Fuller, L. Bennett, J. Roque, W. Sun, S. A. McFarland, *Photochem. Photobiol.* **2019**, *95*, 267–279.

[34] J. Sherwood, J. H. Clark, I. J. S. Fairlamb, J. M. Slattery, *Green Chem.* **2019**, *21*, 2164–2213.

[35] L. Jedinák, R. Zátopková, H. Zemánková, A. Šustková, P. Cankař, *J. Org. Chem.* **2017**, *82*, 157–169.

[36] V. Farina, S. Kapadia, B. Krishnan, C. Wang, L. S. Liebeskind, *J. Org. Chem.* **1994**, *59*, 5905–5911.

[37] L. S. Liebeskind, R. W. Fengl, *J. Org. Chem.* **1990**, *55*, 5359–5364.

[38] A. K. Mengele, S. Kaufhold, C. Streb, S. Rau, *Dalt. Trans.* **2016**, *45*, 6612–6618.

[39] U. Kölle, M. Grützel, *Angew. Chem. Int. Ed.* **1987**, *26*, 567–570.

[40] C. White, A. Yates, P. M. Maitlis, *Inorg. Synth.* **1992**, *29*, 228–234.

[41] S. Kaufhold, L. Petermann, D. Sorsche, S. Rau, *Chem. - A Eur. J.* **2017**, *23*, 2271–2274.

[42] P. V. R. Schleyer, H. Jiao, *Pure Appl. Chem.* **1996**, *68*, 209–218.

[43] J. A. N. F. Gomes, R. B. Mallion, *Chem. Rev.* **2001**, *101*, 1349–1383.

[44] M. G. Pfeffer, C. Pehlken, R. Staehle, D. Sorsche, C. Streb, S. Rau, *Dalt. Trans.* **2014**, *43*, 13307–13315.

[45] S. D. Bergman, D. Reshef, S. Groysman, I. Goldberg, M. Kol, *Chem. Commun.* **2002**,

2, 2374–2375.

[46] H. juan Yu, J. ping Liu, Z. feng Hao, J. He, M. Sun, S. Hu, L. Yu, H. Chao, *Dye. Pigment.* **2017**, *136*, 416–426.

[47] X. S. Ke, Y. Hong, V. M. Lynch, D. Kim, J. L. Sessler, *J. Am. Chem. Soc.* **2018**, *140*, 7579–7586.

[48] R. C. Fortenberry, C. M. Novak, T. J. Lee, P. P. Bera, J. E. Rice, *ACS Omega* **2018**, *3*, 16035–16039.

[49] T. Hatakeyama, S. Hashimoto, S. Seki, M. Nakamura, *J. Am. Chem. Soc.* **2011**, *133*, 18614–18617.

[50] F. H. Herbstein, *Acta Crystallogr. Sect. B Struct. Crystallogr. Cryst. Chem.* **1979**, *35*, 1661–1670.

[51] N. Yoshida, S. Kamiguchi, K. Sakao, R. Akasaka, Y. Fujii, T. Maruyama, T. Iwasawa, *Tetrahedron Lett.* **2020**, *61*, 152033.

[52] Y. Ueda, H. Tsuji, H. Tanaka, E. Nakamura, *Chem. - An Asian J.* **2014**, *9*, 1623–1628.

[53] L. Ademi, E. C. Constable, C. E. Housecroft, M. Neuburger, S. Schaffner, *Dalt. Trans.* **2003**, 3565–4567.

[54] J. E. O'Reilly, P. J. Elving, *J. Am. Chem. Soc.* **1971**, *93*, 1871–1879.

[55] B. Schäfer, H. Görls, S. Meyer, W. Henry, J. G. Vos, S. Rau, *Eur. J. Inorg. Chem.* **2007**, 4056–4063.

[56] J. A. Hopkins, D. Lionetti, V. W. Day, J. D. Blakemore, *Organometallics* **2019**, *38*, 1300–1310.

[57] P. Wintergerst, A. K. Mengele, D. Nauroozi, S. Tschierlei, S. Rau, *Eur. J. Inorg. Chem.* **2019**, *2019*, 1988–1992.

[58] K. Suzuki, A. Kobayashi, S. Kaneko, K. Takehira, T. Yoshihara, H. Ishida, Y. Shiina, S. Oishi, S. Tobita, *Phys. Chem. Chem. Phys.* **2009**, *11*, 9850–9860.

[59] M. Ladwig, W. Kaim, *J. Organomet. Chem.* **1991**, *419*, 233–243.

[60] S. Campagna, F. Puntoriero, F. Nastasi, G. Bergamini, V. Balzani, *Top. Curr. Chem.* **2007**, *280*, 117–214.

[61] M. Wächtler, J. Guthmuller, L. González, B. Dietzek, *Coord. Chem. Rev.* **2012**, *256*, 1479–1508.

[62] C. V. Kumar, J. K. Barton, I. R. Gould, N. J. Turro, J. Van Houten, *Inorg. Chem.* **1988**, *27*, 648–651.

[63] M. Karnahl, S. Krieck, H. Görls, S. Tschierlei, M. Schmitt, J. Popp, D. Chartrand, G. S. Hanan, R. Groarke, J. G. Vos, S. Rau, *Eur. J. Inorg. Chem.* **2009**, *2009*, 4962–4971.

[64] L. Zedler, J. Guthmuller, R. de M. Inês, S. Kupfer, S. Krieck, M. Schmitt, J. Popp, S. Rau, B. Dietzek, I. Rabelo de Moraes, S. Kupfer, S. Krieck, M. Schmitt, J. Popp, S. Rau, B. Dietzek, *Chem. Commun.* **2014**, *50*, 5227–5229.

[65] L. Zedler, A. K. Mengele, K. M. Ziems, Y. Zhang, M. Wächtler, S. Gräfe, T. Pascher, S. Rau, S. Kupfer, B. Dietzek, *Angew. Chemie - Int. Ed.* **2019**, *58*, 13140–13148.

[66] M. Martynow, S. Kupfer, S. Rau, J. Guthmuller, *Phys. Chem. Chem. Phys.* **2019**, *21*, 9052–9060.

[67] C. W. Stark, W. J. Schreier, J. Lucon, E. Edwards, T. Douglas, B. Kohler, *J. Phys.*

Chem. A **2015**, *119*, 4813–4824.

[68] S. Wallin, J. Davidsson, J. Modin, L. Hammarström, *J. Phys. Chem. A* **2005**, *109*, 4697–4704.

[69] N. H. Damrauer, G. Cerullo, A. Yeh, T. R. Boussie, C. V. Shank, J. K. McCusker, *Chemtracts* **1998**, *11*, 621–625.

[70] R. A. Malone, D. F. Kelley, *J. Chem. Phys.* **1991**, *95*, 8970–8976.

[71] J. Olofsson, B. Önfelt, P. Lincoln, *J. Phys. Chem. A* **2004**, *108*, 4391–4398.

[72] M. Kaufmann, C. Müller, A. A. Cullen, M. P. Brandon, B. Dietzek, M. T. Pryce, *Inorg. Chem.* **2021**, *60*, 760–773.

[73] C. Müller, D. Isakov, S. Rau, B. Dietzek, *J. Phys. Chem. A* **2021**, *125*, 5911–5921.

[74] G. E. Shillito, C. B. Larsen, J. R. W. McLay, N. T. Lucas, K. C. Gordon, *Inorg. Chem.* **2016**, *55*, 11170–11184.

[75] J. Schindler, Y. Zhang, P. Traber, J. F. Lefebvre, S. Kupfer, M. Demeunynck, S. Gräfe, M. Chavarot-Kerlidou, B. Dietzek, *J. Phys. Chem. C* **2018**, *122*, 83–95.

[76] Y. Liu, A. Chouai, N. N. Degtyareva, D. A. Lutterman, K. R. Dunbar, *J. Am. Chem. Soc.* **2005**, *127*, 10796–10797.

[77] S. A. Tysoe, R. Kopelman, D. Schelzig, *Inorg. Chem.* **1999**, *38*, 5196–5197.

[78] H. C. Lo, C. Leiva, O. Buriez, J. B. Kerr, M. M. Olmstead, R. H. Fish, *Inorg. Chem.* **2001**, *40*, 6705–6716.

[79] C. L. Pitman, O. N. L. Finster, A. J. M. Miller, *Chem. Commun.* **2016**, *52*, 9105–9108.

[80] K. T. Oppelt, E. Wo, M. Stiftinger, W. Scho, W. Buchberger, *Inorg. Chem.* **2013**, *52*, 11910–11922.

[81] T. Golaś, E. Bojarska, B. Czochralska, *J. Photochem. Photobiol. A Chem.* **1990**, *54*, 333–347.